Biomedicine & Pharmacotherapy 118 (2019) 109323

Contents lists available at ScienceDirect

Biomedicine & Pharmacotherapy

journal homepage: www.elsevier.com/locate/biopha

Original article

Folate-coated, long-circulating and pH-sensitive liposomes enhance doxorubicin antitumor effect in a breast cancer animal model

Juliana de Oliveira Silva[a], Renata Salgado Fernandes[a], Caroline Mari Ramos Oda[a], Tiago Hilário Ferreira[b], Ana Flávia Machado Botelho[c], Marília Martins Melo[d], Marcelo Coutinho de Miranda[e], Dawidson Assis Gomes[e], Geovanni Dantas Cassali[f], Danyelle M. Townsend[g], Domenico Rubello[h], Mônica Cristina Oliveira[a], André Luís Branco de Barros[b,*]

[a] Department Pharmaceutical Products, Faculty of Pharmacy, Universidade Federal de Minas Gerais, Belo Horizonte, Minas Gerais, Brazil
[b] Department of Clinical and Toxicological Analyses, Faculty of Pharmacy, Universidade Federal de Minas Gerais, Belo Horizonte, Minas Gerais, Brazil
[c] Department of Veterinary Medicine, School of Veterinary and Zootechny, Universidade Federal de Goiás, Goiânia, Goiás, Brazil
[d] Department of Veterinary Clinical and Surgery, School of Veterinary, Universidade Federal de Minas Gerais, Belo Horizonte, Minas Gerais, Brazil
[e] Department of Biochemistry and Immunology, Institute of Biological Sciences, Universidade Federal de Minas Gerais, Belo Horizonte, Minas Gerais, Brazil
[f] Department of General Pathology, Institute of Biological Sciences, Universidade Federal de Minas Gerais, Belo Horizonte, Minas Gerais, Brazil
[g] Department of Drug Discovery and Pharmaceutical Sciences, Medical University of South Carolina, USA
[h] Department of Radiology, Molecular Imaging, Interventional Radiology, NeuroRadiology, Medical Physics, Pathology, Biomarkers Unit, Clinical Laboratory, Microbiology Unit, Rovigo & Adria Hospital, Rovigo, Italy

ARTICLE INFO

Keywords:
pH-Sensitive liposome
Doxorubicin
Folic acid
Breast cancer
Long-circulating liposome
Cardiotoxicity

ABSTRACT

Long circulating pH-sensitive liposomes have been shown to effectively deliver doxorubicin (DOX) to tumors and reduce its toxic effects. Folic acid receptors are upregulated in a wide variety of solid, epithelial tumors, including breast cancer. In order to improve liposomal endocytosis and antitumor activity, folic acid has been added to nanoparticles surfaces to exploit overexpression of folate receptors in tumor cells. The purpose of this study was to evaluate the antitumor activity *in vitro* and *in vivo* of long circulating pH-sensitive folate-coated DOX-loaded liposomes (SpHL-DOX-Fol) in a 4T1 breast cancer model system *in vitro* and *in vivo*. Biodistribution studies were performed and *in vivo* electrocardiographic parameters were evaluated. A higher tumor uptake for radiolabeled SpHL-Fol (^{99m}Tc-SpHL-Fol) 4 h after intravenous administration was observed in comparision with non-folate-coated liposomes (^{99m}Tc-SpHL). Antitumor activity showed that SpHL-DOX-Fol treatment led to a 68% growth arrest and drastically reduce pulmonary metastasis foci. Additionally, eletrocardiographic parameters analysis revealed no dispersion in the QT and QTc interval was observed in liposomal treated mice. In summary, this novel multifunctional nanoplatform deomonstrated higher tumor uptake and antitumor activity. SpHL-DOX-Fol represents a drug delivery platform to improve DOX tumor delivery and reduce dose-limiting toxicity.

1. Introduction

Breast cancer is the leading cause of cancer-related deaths among women [1,2]. Doxorubicin (DOX) is an anthracycline based-chemotherapy and is used in the front-line treatment of breast cancer [1]. The mechanism of action of DOX is primarily attributed to the inhibition of human topoisomerase I and II activity. However, DOX treatment also leads to DNA damage and the formation of damaging reactive oxygen species (ROS). These mechanisms of cell injury/ death are non-specific and occur through the activation of p53 dependent apoptosis pathways and autophagy processes in healthy and cancer cells [3,4]. Consequently, DOX induced cell injury/ death extends to off target tissues and is dose-limited by cardiotoxicity [5]. DOX induced cardiomyopathy leads to electrocardiographic (ECG) abnormalities as QT and QTc dispersion. QT interval measures the ventricular repolarization process, and its prolongation is related with heart fibrillation [6].

Liposomes have been used to improve selective drug delivery and consequently reduce DOX induced cardiotoxicity. Our research group

* Corresponding author.
E-mail addresses: albb@ufmg.br, brancodebarros@yahoo.com.br (A.L.B. de Barros).

https://doi.org/10.1016/j.biopha.2019.109323
Received 19 June 2019; Received in revised form 23 July 2019; Accepted 26 July 2019

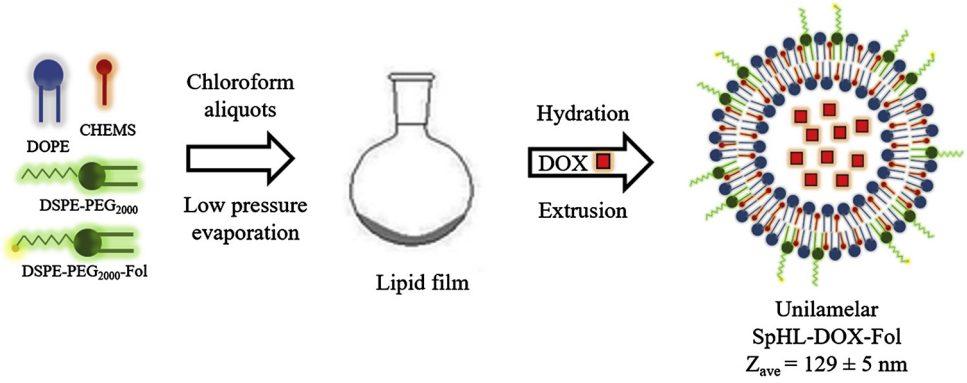

Fig. 1. Schematic illustration of SpHL-DOX-Fol preparation. The size of liposome in figure is merely illustrative.

has utilized long-circulating and pH-sensitive liposomes (SpHL) as a tool to delivery a wide variety of antitumor agents, including DOX, into solid tumors. The delivery of anticancer drugs mediated by SpHL is attributed to the enhanced permeation and retention effect (EPR), leading to enhanced antitumor activity and reduced systemic toxic effects [7–11]. Cellular uptake of SpHL occurs by endocytosis. The low pH of endosomes (˜ pH 5.0) triggers the release of the antitumor drug from the SpHL [12,13]. This pH-responsiveness may be attributed to the presence of dioleoylphosphatidylethanolamine (DOPE) in the liposome bilayer. In an aqueous medium, DOPE molecules are organized into a hexagonal form instead of lamellar structures. The liposome formation with DOPE requires the use of stabilizing agents, usually carboxylated lipids, such as cholesteryl hemisuccinate (CHEMS). In physiological pH, CHEMS is ionized and inserted between the DOPE molecules resulting in electrostatic repulsions between the CHEMS ionized carboxyl groups and the DOPE phosphate groups. Then, the lamellar organization is favorable for spontaneous liposomal formation. The high acidity, lower pH in the endosomal results in the protonation of CHEMS molecules, and consequently, destabilization of the vesicles leads to drug release [7,14–16]. The pH-sensitive behavior is an advantage in several types of organic and inorganic nanoparticles due to the fast drug release in the acidic environment. These nanosystems, as well as pH-sensitive liposomes, were able to delivery DOX to the tumor, with lower systemic toxicity [17–19]. In order to improve liposomal endocytosis, several ligands have been added to the liposomes surface based on overexpressed molecules on the surface of cancer cells [20]. Folate receptor (FR) expression is relatively lower in healthy normal cells; however, FR is overexpressed in more than 40% of tumors, including breast cancer [21]. Thus, folic acid is a promising molecule to coat liposomes to enhance selective cancer cell uptake. Our research group demonstrated these advantages in the use of folate-coated, paclitaxel-loaded pH-sensitive liposomes in *in vitro* as well as *in vivo* assays [22,23]. These studies suggest that, folate-coated, long-circulating and DOX-loaded pH-sensitive liposomes (SpHL-DOX-Fol) may be a promising tool to improve cancer cell uptake of DOX. Therefore, the goal of this study was to evaluate the cytotoxic and antitumor activity of a folate-coated, long-circulatind and pH-sensitive liposomal formulation containing DOX (SpHL-DOX-Fol) using a 4T1 breast tumor as experimental model. Additionally, the biodistribution profile of SpHL-Fol was determined along with blood circulation time. Cardiotoxicity was monitored using electrocardiographic parameters in 4T1 breast tumor-bearing mice following treatment.

2. Material and methods

2.1. Materials

Doxorubicin hydrochloride (DOX) was obtained from 141 ACIC Chemicals (Ontario, Canada). DOPE, distearoylphosphatidylethanolaminepolyethyleneglycol 2000 (DSPE-PEG_{2000}) was purchased from Lipoid GmbH (Ludwigshafen, Germany). Polycarbonate membranes were purchased from Millipore (Burlington, USA). Distearoylphosphatidylethanolaminepolyethyleneglycol 2000 coupled to folate (DSPE-PEG_{2000}-Fol) was purchased from Nanosoft Polymers (Winston-Salem, USA). CHEMSwas purchased from Sigma-Aldrich (St. Louis, USA). Sodium chloride (NaCl) was purchased from Merck (Darmstadt, Germany) and HEPES was purchased from Sigma-Aldrich (St. Louis, USA). Dubelcco's Modified Eagle's Medium (DMEM) was obtained from Sigma-Aldrich (St. Louis, USA). Penicillin, streptomycin and amphotericin B - PSA were purchased from Invitrogen (Carlsbad, USA). Fetal bovine serum (FSB) was obtained from Gibco (Carlsbad, USA). Xylazine solution (Dopaser® 2%) was purchased from Hertape Calier (Juatuba, Brazil). Ketamine hydrochloride solution (Dopalen® 10%) was supplied by Vetbrands Agroline (Campo Grande, Brazil). All reagents were acquired in analytical grade.

2.2. Methods

2.2.1. Liposomes preparation

Liposomes were prepared according to the lipid film hydration method [24], followed by size calibration (Fig. 1). Briefly, chloroform aliquots of DOPE, CHEMS, DSPE-PEG_{2000} (5.8:3.7:0.5 molar ratio, respectively; total lipid concentration was equal to 20 mM) or DOPE, CHEMS, DSPE-PEG_{2000}, and DSPE-PEG_{2000}-Fol (5.8:3.7:0.45:0.05 molar ratio, respectively; total lipid concentration was equal to 20 mM) were transferred to a flask and the solvent was removed at low pressure to prepare SpHL and SpHL-Fol, respectively. Aliquots of 0.1 M NaOH solution were added to lipid film to promote complete ionization of CHEMS molecules, and subsequently, the formation of a lamellar structure. Then, lipid film was hydrated with 300 mM ammonium sulfate solution, at room temperature, under vigorous stirring [9]. The liposomes obtained were calibrated by extrusion using polycarbonate membranes of 0.4 µm, 0.2 µm, and 0.1 µm, 5 cycles per membrane, using the Lipex Biomembranes extruder, Model T001 (Vancouver, Canada). After, ammonium sulfate in the external medium was removed by ultracentrifugation (Ultracentrifuge Optima® L-80XP, Beckman Coulter, Brea, USA) at 150,000 × *g*, 4 °C, for 120 min. The pellet was resuspended with 0.9% (w/v) NaCl solution. Afterward, 2 mg/mL solution of DOX was incubated with SpHL or SpHL-Fol dispersion during 2 h at 4 °C. The non-encapsulated DOX was removed by ultracentrifugation using the same method described above.

2.2.2. Liposomes physicochemical characterization

2.2.2.1. Size, polydispersity index (PDI) and zeta potential. Size and polydispersity index (PDI) were determined by dynamic light scattering (DLS) at 25 °C and an angle of 90°. The zeta potential was determined by electrophoretic mobility associated with DLS. The measurements were performed using Zetasizer NanoZS90 equipment

(Malvern Instruments, Worcestershire, UK). All samples were diluted in 0.9% (w/v) NaCl solution in a ratio of 1:200 and the measurements were performed in triplicate.

2.2.2.2. Determination of the content of DOX. Quantification of DOX was measured by high-performance liquid chromatography (HPLC). The mobile phase was composed of methanol:phosphate buffer pH 3.0 (volume ratio equal to 65:35) with an elution time of 8 min on an ACE® C8, 25 cm x4.6 mm, 5 µm column (Merck, Darmstadt, Germany). The column was kept at room temperature, the injection volume was 20 µL, the flow rate was set at 1.0 mL/min. and the detection was performed with a fluorescence detector model 2475 (Waters Instruments, Milford, MA, USA) with excitation and emission wavelengths of 470 nm and 555 nm, respectively. For quantification of DOX in SpHL-DOX and SpHL-DOX-Fol, the lipid membrane was opened with isopropyl alcohol (volume ratio equal to 1:2), and then the preparation was diluted appropriately in the mobile phase.The amount of DOX was determined before and after ultracentrifugation and the encapsulation percentage (EP) of DOX was calculated according to the following Eq. (1):

$$EP(\%) = ([DOX]\ purified\ liposome/[DOX]\ non-purified\ liposome)\ x\ 100 \quad (1)$$

2.2.2.3. Transmission Electron Microscopy (TEM). Transmission electron microscopy images on the SpHL-DOX-Fol systems were carried out using a negative staining method that provided a complementary morphological evaluation. Briefly, the liposomal formulations were placed on a formvar-coated copper grid and stained with 2% (w/v) phosphotungstic acid solution containing 0.5% (w/v) bovine serum albumin and 0.5% (w/v) saccharose (Monteiro et al., 2018). The stained samples were observed using a FEI Tecnai G2-12 Spirit Biotwin microscope at 120 kV (Centro de Microscopia, Universidade Federal de Minas Gerais, Belo Horizonte, Brazil).

2.2.3. In vitro pH-sensitivity

The pH-sensitivity of SpHL-DOX-Fol was determined by dialysis in HEPES-saline buffer using cellulose membrans with a cutoff size of 12 kDa (Sigma-Aldrich - St. Louis, USA). Dialysis tubes were filled with 250 µL of SpHL-DOX-Fol and incubated in 50 mL of HEPES-saline buffer at pH 7.4 or pH 5.0. The flasks were kept under stirring (200 rpm) at 37 °C in an orbital shaker (IKA KS 4000i - Campinas, Brazil). At 1 h, 4 h, and 24 h, aliquots were collected and DOX concentration inside the dialysis tubes was quantified according to the HPLC method described above.

2.2.4. Cell culture

The 4T1 murine breast cancer cells were grown in DMEM supplemented with 10% (v/v) of FSB and 1% (v/v) of PSA. The cell line was maintained at 37 °C and 5% of CO_2 in a humidified atmosphere.

2.2.4.1. Cytotoxicity assay. 4T1 murine breast tumor cells were seeded in 6-well plates with sterile coverslips (2.5×10^5 cells/well) 24 h before treatment. Cells were exposed to 3µM of DOX, SpHL-DOX, and SpHL-DOX-Fol for 24 h. Following treatment, the cells were washed with PBS buffer and fixed with 3.7% (v/v) formaldehyde and permeabilized with 0.1% (v/v) Triton X-100 solution [25]. After treatment, the cells were fixed with 10% (w/v) trichloroacetic acid (TCA) and after washing, SRB solution was added to the wells. Then, the plate was washed with 1% (v/v) acetic acid to remove non-binding SFB. The protein-bound SRB was solubilized with 10 mM Tris-base solution and the resulting optical density was read at 510 nm in a Spectra Max Plus 384 microplate reader (Molecular Devices – Sunnyvale, USA). A competition assay was also performed in order to confirm the selectivity of SpHL-DOX-Fol. Excessive amounts (1 mM) of free folic acid (FA) was added to the wells 30 min before to SpHL-DOX-Fol addition [21].

2.2.4.2. Confocal microscopy. 4T1 murine breast tumor cells were seeded in 6-well plates with sterile coverslips (2.5×10^5 cells/well) at 24 h before treatment. Cells were exposed to 3µM of DOX, SpHL-DOX, and SpHL-DOX-Fol for 24 h. After, the treatments were withdrawn and wells were washed with PBS buffer. Cells were fixed with 3.7% (v/v) formaldehyde and permeabilized with 0.1% (v/v) Triton X-100 solution [26]. Cell membranes and nuclei were labeled with fluorescent probes Cholera toxin B subunit-Alexa Fluor® 647 (Invitrogen - Carlsbad, USA) and Hoechst 33258 (Thermo Fisher Scientific - Waltham, USA), respectively. The coverslips were washed with PBS and slides were assembled using Prolong Gold Antifade Reagent (Thermo Fisher Scientific - Waltham, USA). Cells were analyzed in *"Centro de Aquisição e Processamento de Imagens da UFMG (CAPI/UFMG)"* using the LSM 880 microscope with Airyscan detector (ZEISS - Oberkochen, Germany). For image acquisition, it was used 40x objective lens. The lasers used were: Diode 405 nm (excitation of Hoechst 33258), Argonium 488 nm (excitation of DOX) and HeNe 633 nm (excitation of Alexa Fluor®647). The images were processed using the ZEN Blue Edition software version 2.3 lite (ZEISS - Oberkochen, Germany).

2.2.5. In vivo studies

2.2.5.1. Animals. Female BALB/c mice aged 6–8 weeks (18–22 g) were obtained from *"Centro de Bioterismo da UFMG (CEBIO/UFMG)"*. Mice were kept on ventilated shelves with light and temperature control and with free access to food and water. All studies were approved by *"Comitê de Ética no Uso de Animais da UFMG (CEUA/UFMG)"* under protocol number CEUA 134/2018.

2.2.5.2. Radiolabeling of liposomes. Radiolabeling of the liposomes occurred in the presence of 0.05 mM of DSPE-PEG_{2000}-DTPA. The compound was synthesized as previously described [27]. In a flask, 250 µL of SpHL or SpHL-Fol was added followed by 200 µg of $SnCl_2{\cdot}2H_2O$ in acid solution (2 mg/mL) and the pH was adjusted to 7.4. Then, 0.9% (w/v) NaCl solution containing approximately 37 MBq of sodium pertechnetate ($Na^{99m}TcO_4$) was added to the sealed flask and the mixture was kept at room temperature for 30 min. Radiochemical purity analyses were performed by thin layer chromatography (TLC) using Whatman paper (Sigma-Aldrich - St. Louis, USA) and acetone as mobile phase to quantify free $^{99m}TcO_4^-$. The radioactivity was determined by a gamma counter (Wallac Wizard 1470–020 Gamma Counter - Waltham, USA). The solution was purified from $^{99m}TcO_2$ using a 0.22 µm syringe filter [27].

2.2.5.3. In vitro radiolabeling stability. TLC was used to estimate the stability of ^{99m}Tc-SpHL and ^{99m}Tc-SpHL-Fol in the presence of 0.9% (w/v) NaCl at room temperature or plasma at 37 °C. For plasma stability, 90 µL of the liposomes were incubated with 1.0 mL of fresh mice plasma, under agitation, at 37 °C. Radiochemical stability was determined on samples taken up at 0, 30 min, 1, 2, 4, 6, and 24 h after incubation.

2.2.5.4. Blood clearance. ^{99m}Tc-SpHL and ^{99m}Tc-SpHL-Fol (3.7 MBq in 100 µL) were administrated to healthy female BALB/c mice (n = 7) by tail vein injection. Mice were anesthetized using ketamine and xylazine (80 mg/kg and 15 mg/kg, respectively) and small blood samples were collected from the tail at 1, 5, 10, 15, 30, 60, 90, 120, 240, 360 and 1440 min post-injection. Blood samples were weighted and the radioactivity associated with each sample was measured using a gamma counter. A decay curve was plotted using the percentage of injected dose per gram (%ID/g) as a function of time.

2.2.5.5. Biodistribution studies. The tumor 4T1 cells were injected in the right flank of female BALB/c mice (2.5×10^6 cell/animal). ^{99m}Tc-SpHL and ^{99m}Tc-SpHL-Fol (3.7 MBq in 100 µL) were administrated to tumor-bearing mice (n = 7) by the tail vein after the tumors reached close to

100 mm^3. The mice were anesthetized using ketamine and xylazine (80 mg/kg and 15 mg/kg, respectively). Tissue distribution was assessed at 4 and 24 h post-injection. The following organs were harvested, weighed and analyzed by a gamma counter: liver, spleen, kidneys, stomach, lungs, muscle, thyroid, intestine and tumor. Data were shown as %ID/g of tissue and the tumor-to-muscle ratio was calculated.

2.2.5.6. Antitumor activity. Seven days after tumor induction, when tumor volume reached ~100 mm^3, animals were randomly divided into 4 groups (n = 7), namely SpHL (control group), DOX, SpHL-DOX, or SpHL-DOX-Fol. Animals received a dose of 5 mg/kg, every three days, reaching a cumulative dose of 20 mg/kg. Tumor dimensions were measured using a caliper every two days. Mice body weight was measured at the same time. The tumor volume (V) was calculated by the following Eq. (2), where d_1 and d_2 are the smaller and larger diameter, respectively.

$$V = (d_1)^2 x\, d_2\, x\, 0.5 \quad (2)$$

At five days after last treatment dose, mice were anesthetized, using ketamine and xylazine (80 mg/kg and 15 mg/kg, respectively), and then, euthanized. Tumor, lungs, heart, kidneys, and liver were collected to histopathological analysis. The relative tumor volume (RTV) and inhibition ratio (IR) was calculated at the end of the study by the following Eqs. (3, 4):

$$RTV = \frac{Tumor\ volume\ (last\ day)}{Tumor\ volume\ (first\ day)} \quad (3)$$

$$IR = 1 - \left(\frac{RTV\ of\ drug - treated\ group}{RTV\ of\ control\ group} \right) \quad (4)$$

2.2.5.7. Histopathological analysis. Tumor, lungs, heart, kidneys, and liver were collected (n = 5) and fixed in 10% buffered formalin for 24 h–48 h. Then, samples were dehydrated in alcohol and embedded in paraffin blocks. 4 µm sections were obtained and stained with hematoxylin and eosin (H&E). Trained pathologists evaluated the slides and images were captured by a camera connected to an Olympus BX-40 optical microscope (Olympus - Tokyo, Japan). The number of metastasis foci in lungs were counted in individual animals and expressed by the following semi-quantitative score: 0, no metastasis detected; +, 1–3 metastatic foci; ++, 4–7 metastatic foci; +++, 8–10 metastatic foci; ++++, > 10 metastatic foci in lungs [28].

2.2.5.8. Electrocardiographic analysis. The evaluation of *in vivo* cardiac electrophysiology was performed by electrocardiographic (ECG) records analysis. The records were acquired from tumor-bearing animals (n = 5) before administration, as a baseline, and 24 h after each treatment. The records were acquired with a six-channel electrocardiograph (ECG-PC version 2.07®; Tecnologia Eletrônica Brasileira (TEB) - Belo Horizonte, Brazil). All animals were exposed to superficial anesthesia with isoflurane at a concentration of 2.0 to 2.5% for induction and 1.0 to 1.5% for maintenance using a Vetcase Anesthesia apparatus (Brasmed® - Paulínia, Brazil). Mice were placed in a dorsal recumbence position and four alligator clip electrodes were attached to the skin in the forelimbs and hindlimbs [29]. All procedures were performed in a quiet room in order to minimize stress.

ECGs were performed and analyzed by the same veterinary according to standard methods. Tracings were recorded in six leads of the frontal plane, with 50 mm/s of velocity and sensitivity of 1cm = 2 mV (2 N). In each tracing three segments, containing five beats (DII shunt) were selected for quality (clean baseline with no artifacts). Mean values for heart rate (HR) and length of P-QRS-T deflections were determined. The parameters evaluated were: QT interval (measured from the beginning of the QRS complex to the end of the T–wave), PR interval (interval between the beginning of the P-wave and the end of the R-wave), QRS complex (measured from the beginning of the Q-wave to the end of the S-wave) and the RR interval (interval between two successive R-waves and used for the determination of heart rate HR = 60/RR). Corrected QT (QTc) values were obtained from the Fridericia formulae ($QTc = QT/(RR)^{1/3}$). The morphology patterns were evaluated in every lead, and P-QRS-T measurements were conducted in DII shunt.

2.2.6. Statistical analysis

Data were expressed as the mean ± standard deviation (SD). The normality and homoscedasticity of the variables were verified by D'Agostino and Barlett tests, respectively [30]. Differences between the experimental groups were assessed using one-way ANOVA analysis of variance followed by Tukey's test. For all analyses, the 95% confidence interval was adopted and the differences were considered significant when the P-value was < 0.05 ($P < 0.05$). Data were evaluated with GraphPad Prism software (version 5.00, La Jolla, USA).

3. Results

3.1. Physicochemical characterization of liposomes

The physicochemical properties of the liposomes (SpHL, SpHL-Fol, SpHL-DOX, and SpHL-DOX-Fol) are shown in Table 1. No significant differences were observed between SpHL and SpHL-Fol in size, PDI and zeta potential. The encapsulation method was suitable reaching almost 100% of encapsulation percentage. In addition, the DOX encapsulation and functionalization processes did not alter the liposomes size, zeta potential, and PDI. In addition, the TEM analysis of SpHL-DOX-Fol showed predominantly unilamellar structures close to spheric form and smaller than 200 nm (Fig. 2).

3.2. In vitro pH-sensitivity

In vitro pH-sensitivity of SpHL-DOX-Fol was evaluated as a function of time at different pH (7.4 and 5.0). Results are shown in Table 2. After 4 h, SpHL-DOX-Fol in acidic medium showed a higher percent release relative to neutral pH ($P < 0.05$). Additionally, at 24 h, 53.6 ± 5.7% of DOX was released from SpHL-DOX-Fol at pH 5.0, while at pH 7.4 only 21.5 ± 3.9% was released in the medium.

3.3. Cell viability and confocal microscopy

Cell viability was evaluated to compare forumulations of SpHL and SpHL-Fol (blank liposomes), free DOX, SpHL-DOX, SpHL-DOX-Fol, and SpHL-DOX-Fol + free FA after 48 h exposure. Cytotoxicity was not observed in cells treated with SpHL or SpHL-Fol, suggesting the vehicle was not toxic. Consequently the half-maximal inhibitory concentration (IC_{50}) for blank formulations was not calculated for the controls. For drug-loaded nanoparticles (DOX, SpHL-DOX, and SpHL-DOX-Fol) there

Table 1
Physicochemical characterization of SpHL, SpHL-Fol, SpHL-DOX, and SpHL-DOX-Fol.

	Size (nm)	Polydispersity Index (PDI)	Zeta Potential (mV)	Encapsulation Percentage (%)
SpHL	126 ± 4	0.09 ± 0.03	−3.7 ± 1.3	–
SpHL-Fol	130 ± 7	0.07 ± 0.03	−5.0 ± 1.2	–
SpHL-DOX	123 ± 6	0.07 ± 0.01	−3.3 ± 0.7	100.9 ± 1.8
SpHL-DOX-Fol	129 ± 5	0.06 ± 0.03	−4.2 ± 1.4	97.6 ± 3.8

Data are expressed by the mean (n = 3) ± standard deviation of the mean. All data were analyzed by one-way ANOVA analysis of variance followed by Tukey's post-test.

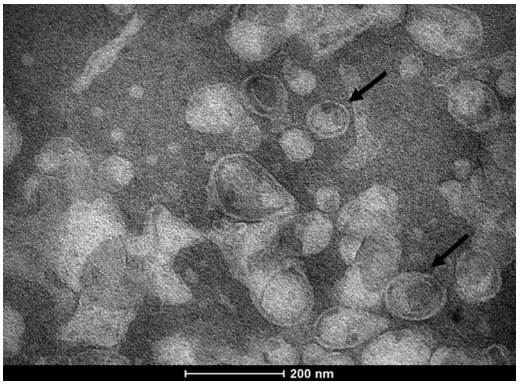

Fig. 2. TEM photomicrographs of SpHL-DOX-Fol. The black arrows indicate unilamellar liposomes.

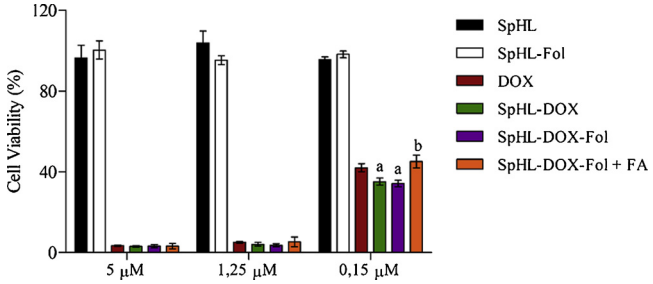

Fig. 3. Cytotoxicity of the treatments SpHL, SpHL-Fol, free DOX, SpHL-DOX, SpHL-DOX-Fol, and SpHL-DOX-Fol with FA excess against 4T1 murine breast tumor cells. Data are expressed by the mean ± standard deviation of the mean of independent experiments (n = 3). All data were analyzed by one-way ANOVA analysis of variance followed by Tukey's post-test. [a]Represents statistical differences ($P < 0.05$) between DOX and SpHL-DOX or SpHL-DOX-Fol treatments. [b]Represents statistical differences ($P < 0.05$) between SpHL-DOX-Fol + FA and SpHL-DOX-Fol treatments at the same dose.

was a dose-dependent effect on cytotoxicity (Fig. 3). The IC_{50} value for DOX, SpHL-DOX, and SpHL-DOX-Fol treatments were 0.131 ± 0.038 μM, 0.097 ± 0.023 μM and 0.099 ± 0.016 μM, respectively. Although no statistical differences ($P > 0,05$) were observed among the IC_{50} values, at low concentration (0.15μM), liposomes showed higher cytotoxicity than the free drug. Furthermore, Fig. 3 shows that cells pretreatment with free FA (1 mM) resulted in significant ($P < 0.05$) decrease of the SpHL-DOX-Fol cytotoxicity at low concentrations (0.15μM) and significant increase in IC_{50} value was observed (0.143 ± 0.039 μM). Confocal microscopy images are shown in Fig. 4. The intracellular DOX localization was nuclear, colocalizing with DNA staining for all drug-treated cells (Free DOX, SpHL-DOX, SpHL-DOX-Fol), suggesting efficient DOX delivery.

3.4. Radiolabeling of liposomes and in vitro stability

^{99m}Tc-SpHL and ^{99m}Tc-SpHL-Fol were efficiently prepared and reproducible. Radiochemical purity was 98.6 ± 0.4% and 99.8 ± 0.1%, respectively. The radiolabeling process did not lead to modification of the liposomes physicochemical parameter as size, PDI, and zeta potential. In addition, ^{99m}Tc-SpHL and ^{99m}Tc-SpHL-Fol showed great *in vitro* stability indicating their feasibility to *in vivo* studies (Fig. 5).

3.5. Blood circulation time

The pharmacokinetic parameters of ^{99m}Tc-SpHL and ^{99m}Tc-SpHL-Fol after intravenous administration in healthy BALB/c mice was evaluated. A biphasic clearance profile for ^{99m}Tc-SpHL was observed. Specifically, the compound showed a fast half-life of 8.3 min and a long half-life of 189.4 min. Similar parameters were observed for administration of ^{99m}Tc-SpHL-Fol with a fast half-life of 6.3 min and long half-life of 226.9 min.

3.6. Biodistribution studies

The biodistribution profile of ^{99m}Tc-SpHL and ^{99m}Tc-SpHL-Fol in mice are shown in Fig. 6A and B. Both liposomes formulations present high uptake from the mononuclear phagocyte system (MPS), such as liver and spleen, as expected for many nanosystems [31]. Renal uptake was also noted. *In vitro* stability data were confirmed since no significant uptake in stomach and thyroid at 4 h and 24 h were observed. The tumor-to-muscle ratio was observed at 4 h post-injection, a higher ($P < 0.05$) tumor-to-muscle ratio for ^{99m}Tc-SpHL-Fol (2.21) than ^{99m}Tc-SpHL (1.28) (Fig. 6C). Thus, the tumor-to-muscle ratio are greater than 1.5% and almost two-fold higher for folate-coated liposome treatment in comparision with non-folate-coated liposome formulation. This ratio indicates a suitable distinction between tumor and healthy tissues [15]. It is noteworthy that no difference of the tumor-to-muscle ratio was observed in either formulations at 24 h, indicating that active targeting might be important in the first hours. However, at longer time intervals, the EPR effect seems to regulate the tumor uptake.

3.7. Antitumor activity

The antitumor activity was evaluated *in vivo* using a breast cancer model. Significant differences in the antitumor activity were observed among SpHL treatment (control group) verses treatments with DOX, SpHL-DOX or SpHL-DOX-Fol ($p < 0.05$), Fig. 7. These results show that SpHL-DOX-Fol treatment was the most effective. Tumor volume data were confirmed by the RTV values (Fig. 7B). The IR for free DOX, SpHL-DOX, and SpHL-DOX-Fol was 37%, 56%, and 68%, respectively. In addition, there is no significant difference in body weight loss for all drug-treated groups before euthanasia (Fig. 7C).

3.8. Histopathological analysis

Both tumor and normal tisssues were evaluated by histology for necrosis and metastasis. Histological analysis of breast cancer tumors are presented in Fig. 8. Treatment with free DOX, SpHL-DOX or SpHL-DOX-Fol, showed extensive necrosis due to DOX-induced cell death (Fig. 8B–D, respectively). However, SpHL-DOX-Fol-treated tumor (Fig. 8D) presented more extensive necrosis compared to other formulations. Lung and liver tissues were evaluated for the appearance of

Table 2
Release profile of SpHL-DOX-Fol at pH 7.4 and pH 5.0 at different times.

	pH 7.4			pH 5.0		
Time	1 h	4 h	24 h	1 h	4 h	24 h
Release (%)	11.0 ± 1.7	22.4 ± 3.2[a]	21.5 ± 3.9[a]	11.6 ± 2.9	42.3 ± 7.9[ab]	53.6 ± 5.7 [ab]

[a] Represents statistical differences ($P < 0.05$) between 1 h and 4 h or 24 h at the same pH. [b]Represents statistical differences ($P < 0.05$) between pH 7.4 and pH 5.0 at the same time. Data are expressed by the mean (n = 3) ± standard deviation of the mean. All data were analyzed by one-way ANOVA analysis of variance followed by Tukey's post-test.

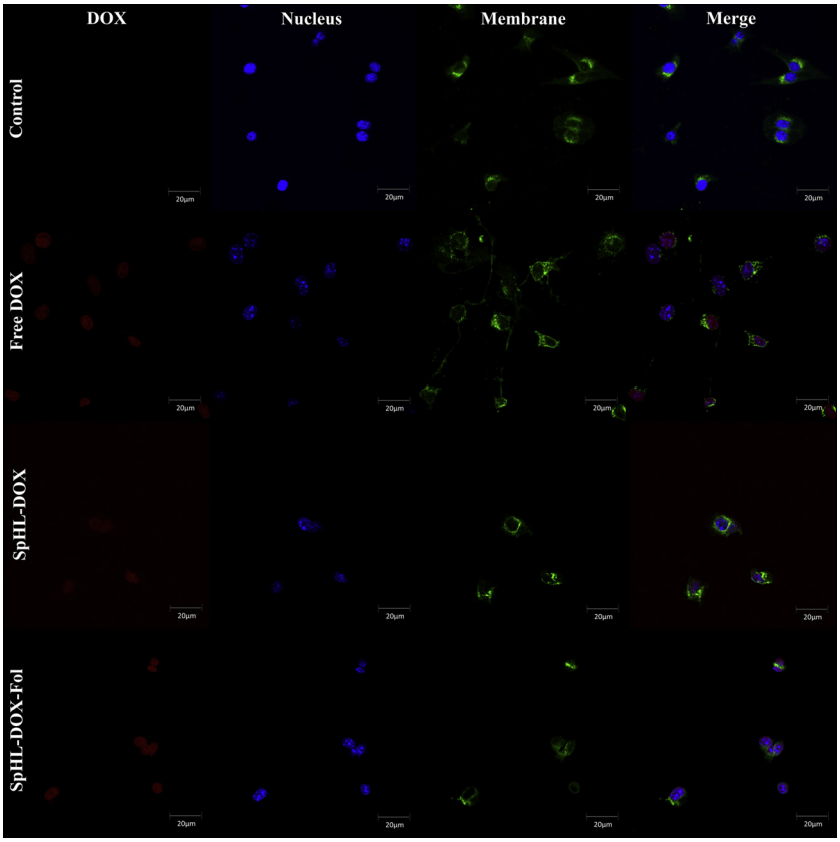

Fig. 4. Confocal microscopy images of 4T1 murine breast tumor cells after 24 h-incubation with free DOX, SpHL-DOX, or SpHL-DOX-Fol treatments (DOX concentration 3μM). Nucleus in blue, cell membranes in green, DOX in red. Amplification of 40×.

metastases (Fig. 9). 4T1 tumors are aggressive and all treatment groups presented metastatic foci in both organs. However, in lungs, SpHL-DOX-Fol treated group exhibited fewer metastatic foci in a semi-quantitative comparison with SpHL, DOX, and SpHL-DOX-treated groups, Table 3.

In order to evaluate the DOX induced cardiotoxicity, cardiac muscle photomicrographs were evaluated (Fig. 10). Morphological changes were observed in all animals receiving DOX, SpHL-DOX, or SpHL-DOX-Fol treatments (Fig. 10B–D, respectively). These photomicrographs presented focal areas of discreet cardiomyocytes vacuolization and degenerative hyalinization evidence. However, no significant differences in the extent of lesions were observed. Morphological changes were not observed in kidney photomicrographs analysis (data not shown).

3.9. Electrocardiographic analysis

Electrocardiographic analysis (ECG) of drug treated, tumor bearing mice are shown in Fig. 11 and Table 4. In QT interval dispersion analysis, significant prolongation ($P < 0.05$) of the QT interval was observed only in DOX-treated animals (100 ± 18 ms) after administraton of the fourth dose compared to baseline (76 ± 7 ms). In addition, significant prolongation ($P < 0.05$) of the QT interval was observed in comparison with SpHL-DOX-treated animals (84 ± 10 ms) or SpHL-DOX-Fol-treated animals (90 ± 5 ms) at same dose (Fig. 11A). Thus, no dispersion in the QT interval was observed in liposome-treated mice. As expected, this behavior was also observed to QTc interval analysis (Fig. 11B). The QRS complex, PR interval, and HR did not show any changes compared to baseline for all treatment groups containing DOX (Table 4).

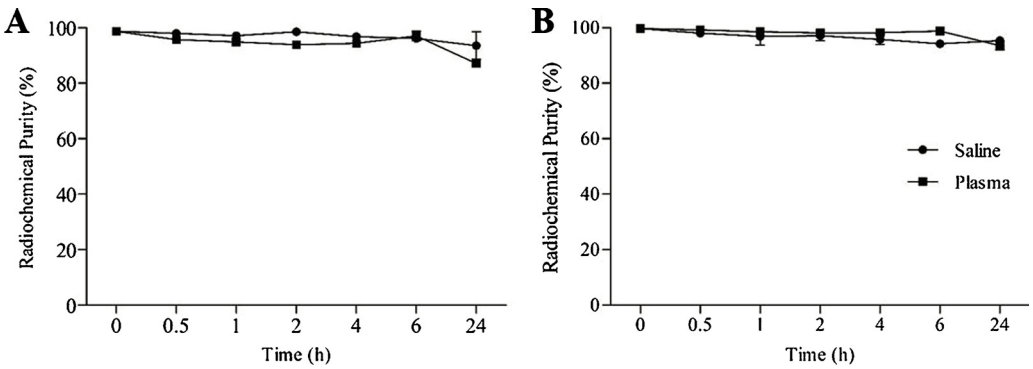

Fig. 5. *In vitro* stability of ^{99m}Tc-SpHL (A) and ^{99m}Tc-SpHL-Fol (B) as a function of the time in the presence of saline at room temperature and plasma at 37 °C. Data are expressed by the mean ± standard deviation of the mean (n = 3).

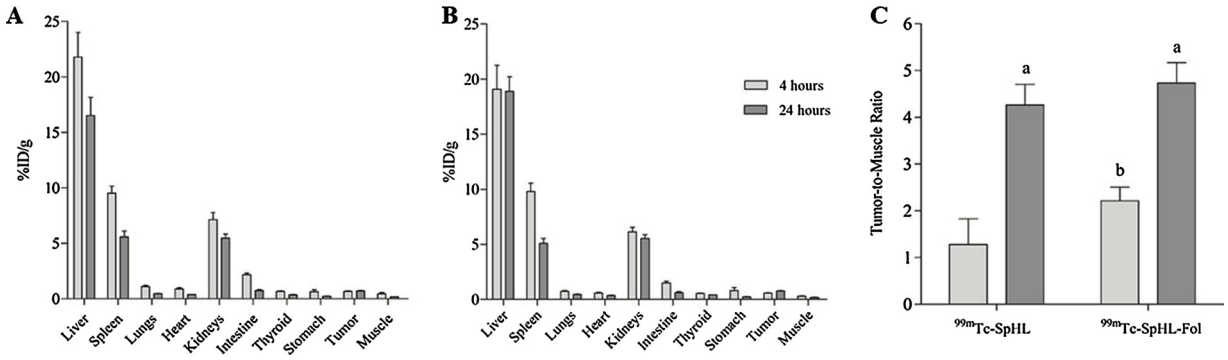

Fig. 6. Biodistribution profile of ^{99m}Tc-SpHL (A) and ^{99m}Tc-SpHL-Fol (B) after intravenous administration in 4T1 breast tumor-bearing female BALB/c mice at 4 h and 24 h. (C) Tumor-to-muscle ratio for ^{99m}Tc-SpHL and ^{99m}Tc-SpHL-Fol. Data are expressed by the mean ± standard deviation of the mean (n = 7). Tumor-to-muscle data were analyzed by one-way ANOVA analysis of variance followed by Tukey's post-test. [a]Represents statistical differences ($P < 0.05$) between 4 h and 24 h for ^{99m}Tc-SpHL or ^{99m}Tc-SpHL-Fol treatments. [b]Represents statistical differences ($P < 0.05$) between ^{99m}Tc-SpHL and ^{99m}Tc-SpHL-Fol at 4 h treatments.

4. Discussion

Folate-coated nanoparticles, including pH-sensitive liposomes, have been studied extensively in the last years as an efficient drug delivery system. The use of folate-coated nanoparticles is based on folate receptor overexpression in several cancer cells, including breast cancer, which enhance cell uptake of nanoparticles and antitumor activity [12,23,32–34]. In this study, folate-coated, long-circulating and pH-sensitive liposomes containing DOX (SpHL-DOX-Fol) were prepared and characterized. Small, uniform, and unilamellar liposomes were prepared (100–200 nm) with efficient DOX encapsulation. Small particle size is associated with longer blood circulation [35]. The pH-sensitivity and DOX release profile was preserved, despite the surface functionalization, as described previously [36]. SpHL-Fol and SpHL-DOX-Fol presented neutral zeta potential due to the presence of DSPE-PEG_{2000} in the liposome lipid composition. The presence of PEG chains on the surface of liposome produces a hydrophilic layer and reduces the electrophoretic mobility generating zeta potential close to neutrality. In addition, PEG chains protect the vesicles from aggregation/fusion, and thus, confer stability and promote *in vivo* prolonged circulation [37,38]. In this context, blood clearance for ^{99m}Tc-SpHL and ^{99m}Tc-SpHL-Fol showed long distribution time (189 and 227 min, respectively). Our results are comparable with previous studies from our research group in which DOX-loaded SpHL and paclitaxel-loaded SpHL presented similar blood circulation time [8,23].

The pharmacokinetic properties of liposomes show long-circulating times which is proposed to confer more passages through the tumor tissue, improving the tumor accumulation of nanoparticles in the tumor. Tumor growth promotes irregular blood vessel formation, with larger pores than normal tissue vasculature favoring EPR effect and liposome extravasation [39]. In the tumor microenvironment, folate-coated nanosystems, including liposomes, were quickly taken up by 4T1 tumor cells [32,40,41] as shown in tumor-to-muscle ratio results at 4 h post-administration of ^{99m}Tc-SpHL-Fol and ^{99m}Tc-SpHL. In this context, ^{99m}Tc-SpHL-Fol could be a promising tool to deliver DOX to the over-expressed folate-receptor tumor, as 4T1 murine breast tumor.

In vitro studies using 4T1 breast tumor cells demonstrated the DOX uptake concentrated in the nucleus [42]. Moreover, cytotoxicity of DOX-treated group was similar to the SpHL-DOX and SpHL-DOX-Fol-treated groups. Despite the modest results observed in cytotoxicity assay, it was demonstrated the influence of folate receptors in the cytotoxicity of SpHL-DOX-Fol, as showed in the competition assay. This

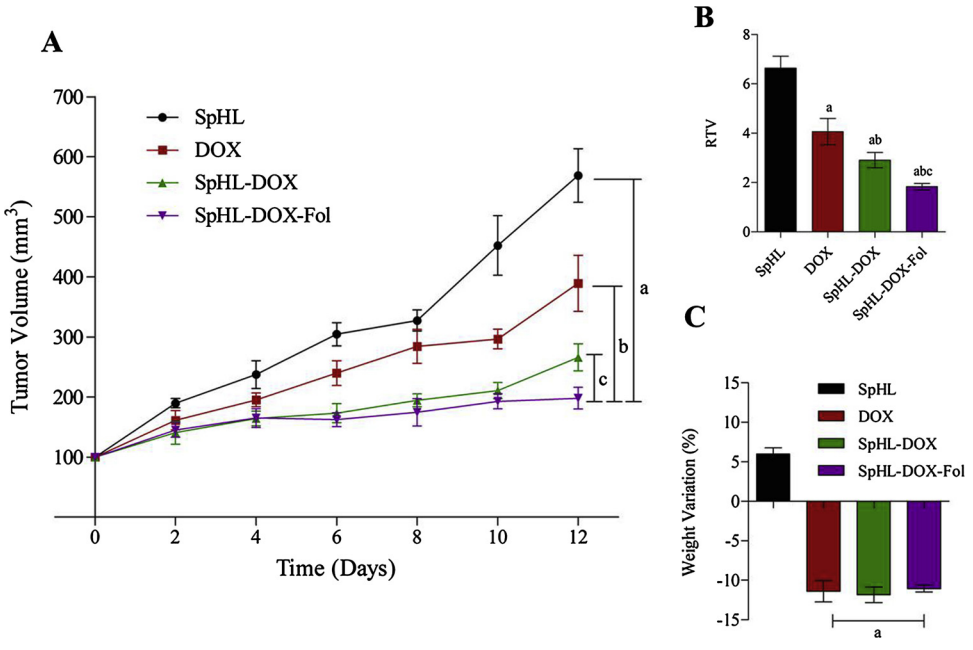

Fig. 7. (A) Antitumor effect of SpHL (control group), DOX, SpHL-DOX, and SpHL-DOX-Fol on the growth of 4T1 breast tumor-bearing female BALB/c mice. Each treatment was intravenously administered 4 times, every 3 days, at dose of 5 mg/kg. Data are expressed by the mean ± standard deviation of the mean (n = 7). Growth curves were analyzed by regression. [a]Represents statistical differences ($P < 0.05$) between SpHL and SpHL-DOX-Fol treatments. [b]Represents statistical differences ($P < 0.05$) between DOX and SpHL-DOX treatments. [b]Represents statistical differences ($P < 0.05$) between SpHL-DOX and SpHL-DOX-Fol treatments. (B) RTV analysis of theSpHL (control group), DOX, SpHL-DOX, and SpHL-DOX-Fol treatments. Data are expressed by the mean ± standard deviation of the mean (n = 7). [a]Represents statistical differences ($P < 0.05$) between DOX, SpHL-DOX or SpHL-DOX-Fol, and SpHL treatments. [b]Represents statistical differences ($P < 0.05$) between DOX and SpHL-DOX or SpHL-DOX-Fol treatments. [c]Represents statistical differences ($P < 0.05$) between SpHL-DOX and SpHL-DOX-Fol treatments. (C) Body weight variation percentage between D0 and D12. Data are expressed by the mean ± standard deviation of the mean (n = 7). [a]Represents statistical differences ($P < 0.05$) between DOX, SpHL-DOX or SpHL-DOX-Fol, and SpHL treatments.

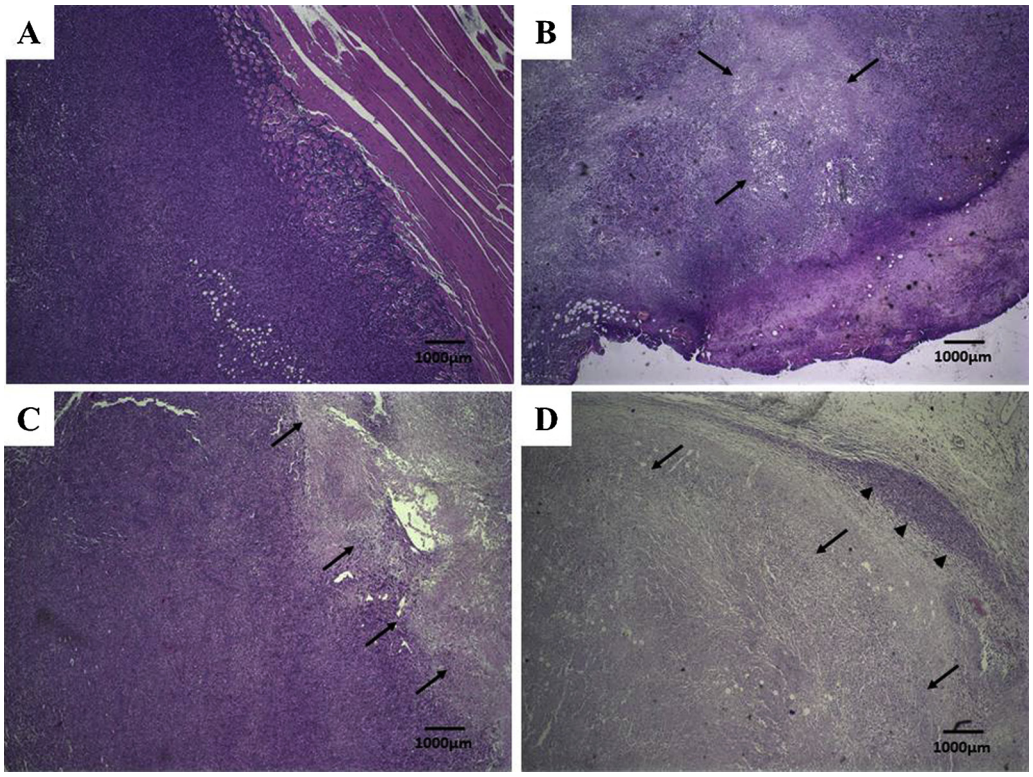

Fig. 8. Histological sections of primary tumor from 4T1 breast tumor-bearing female BALB/c mice treated with SpHL, DOX, SpHL-DOX, or SpHL-DOX-Fol stained by hematoxylin & eosin. (A) SpHL-treated primary tumor. (B) DOX-treated primary tumor. (C) SpHL-DOX-treated primary tumor. (D) SpHL-DOX-Fol-treated primary tumor. The black arrows indicate tumor necrosis areas. The black head arrows indicate tumor area. Amplification of 2 × .

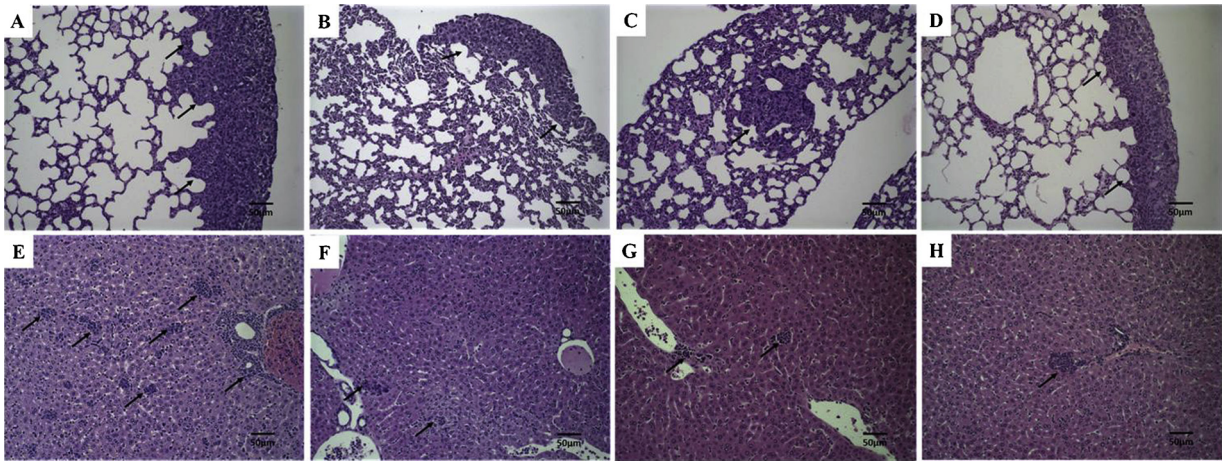

Fig. 9. Histological sections of lungs and liver from 4T1 breast tumor-bearing female BALB/c mice treated with SpHL, DOX, SpHL-DOX, or SpHL-DOX-Fol stained by hematoxylin & eosin. (A) SpHL lungs. (B) DOX, lungs. (C) SpHL-DOX, lungs. (D) SpHL-DOX-Fol, lungs. (E) SpHL-, liver. (F) DOX, liver. (G) SpHL-DOX, liver. (H) SpHL-DOX-Fol, liver. The black arrows indicate metastatic foci. Amplification of 20 × .

Table 3
Number of metastatic foci in the lungs of 4T1 tumor-bearing female BALB/c mice treated with SpHL, DOX, SpHL-DOX or SpHL-DOX-Fol. Each treatment was intravenously administered 4 times, every 3 days, at a dose of 5 mg/kg.

		SpHL	DOX	SpHL-DOX	SpHL-DOX-Fol
Score	Animal 1	+ +	+	+	0
	Animal 2	0	+	+	0
	Animal 3	+	+ +	+	0
	Animal 4	+ + +	0	0	+
	Animal 5	+ +	+	+	0

Data were expressed by score: 0, no metastasis detected; +, 1–3 metastatic foci; + +, 4–7 foci; + + +, 8–10 foci; + + + +, > 10 metastatic foci in lungs.

behavior in competition assay and cytotoxicity were observed previously for different nanosystems delivering antitumor agents [21,32,40].

The 4T1 breast tumor-bearing BALB/c mouse model is a commonly used experimental animal model to mimic late-stage (IV) human breast cancer. The 4T1 breast tumor progresses with primary tumor growth and metastasis in organs, such as, lungs, liver, bones, and brain [28,43]. Our results demonstrated fast tumor growth in SpHL-treated mice (control group) and extensive metastasis foci in lungs and liver. DOX treatment is highly active against 4T1 breast tumor cells, however, the DOX encapsulation in liposomes may enhance its antitumor activity and reduce metastasis occurrence [41,44–46]. Due to FR overexpression in 4T1 breast tumor cells, SpHL-DOX-Fol reduced the tumor growth by nearly 70% and diminished the number and size of metastatic foci in lungs. Comparable tumor growth inhibition was previously reported to

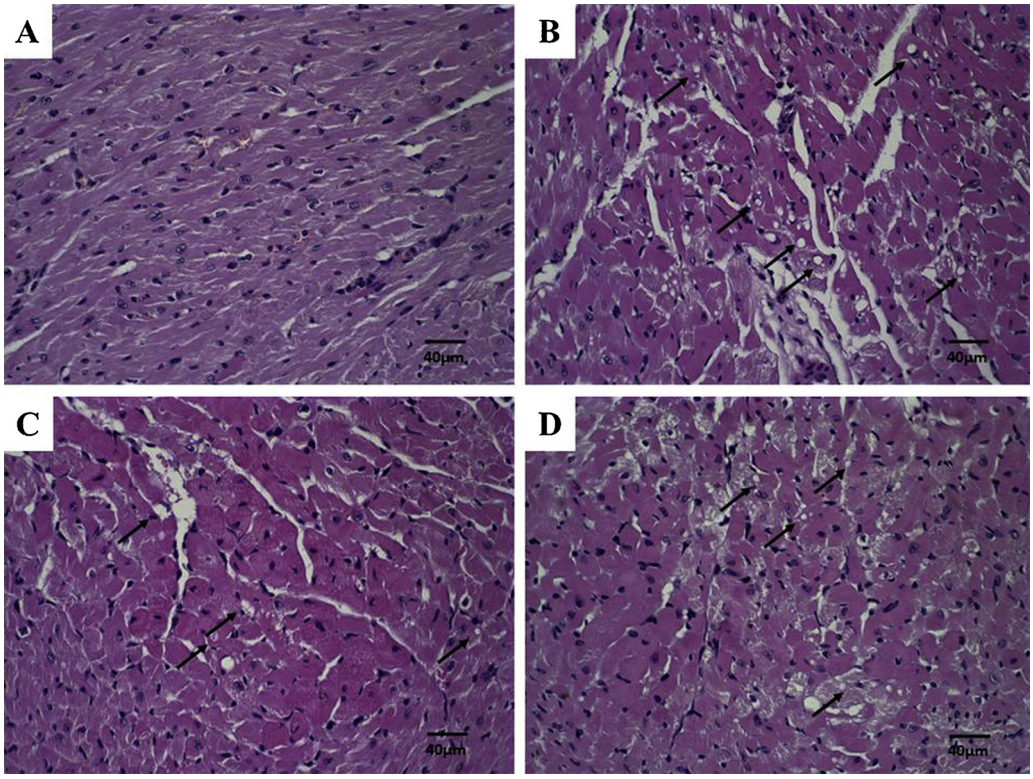

Fig. 10. Histological sections of heart from 4T1 breast tumor-bearing female BALB/c mice treated with SpHL, DOX, SpHL-DOX, or SpHL-DOX-Fol stained by hematoxylin & eosin. (A) SpHL. (B) DOX (C) SpHL-DOX (D) SpHL-DOX-Fol. The black arrows indicate vacuoles in cardiomyocytes. Amplification of 40 × .

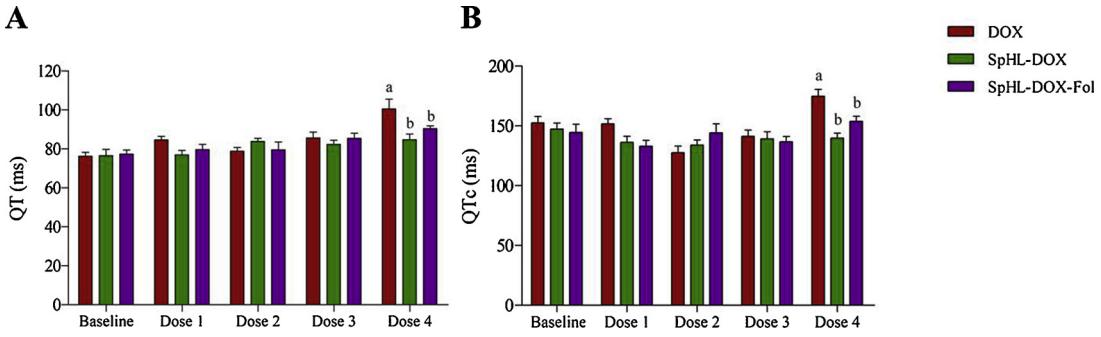

Fig. 11. Electrocardiographic parameters of female 4T1 breast tumor-bearing BALB/c mice treated with DOX, SpHL-DOX, or SpHL-DOX-Fol. Each treatment was intravenously administered 4 times, every 3 days, at a dose of 5 mg/kg. (A) QT interval. (B) QTc interval. Data are expressed as the mean ± standard deviation of the mean (n = 7). All data were analyzed by one-way ANOVA analysis of variance followed by Tukey's post-test. [a]Represents statistical differences ($P < 0.05$) between baseline and DOX treatment after administration of the dose 4. [b]Represents statistical differences ($P < 0.05$) between DOX and SpHL-DOX or SpHL-DOX-Fol treatments after administration of the dose 4.

Table 4
Evaluation of electrocardiographic parameters of 4T1 breast tumor-bearing female BALB/c mice treated with DOX, SpHL-DOX, or SpHL-DOX-Fol. Each treatment was intravenously administered 4 times, every 3 days, at a dose of 5 mg/kg.

Parameter	Dose	DOX	SpHL-DOX	SpHL-DOX-Fol
Heart Rate (beat/min)	Baseline	475 ± 59	411 ± 71	438 ± 29
	After Dose 4	433 ± 54	470 ± 61	457 ± 28
PR Interval (ms)	Baseline	32 ± 4	35 ± 5	34 ± 8
	After Dose 4	33 ± 4	33 ± 3	32 ± 4
QRS Complex (ms)	Baseline	40 ± 7	41 ± 4	44 ± 4
	After Dose 4	48 ± 8	47 ± 7	50 ± 5

Data are expressed by the mean ± standard deviation of the mean (n = 5). All data were analyzed by one-way ANOVA analysis of variance followed by Tukey's post-test.

folate-coated liposomes highlighting the efficiency of using folate-targeting [47]. In addition, the histological analysis of the primary tumor showed greater necrosis areas in SpHL-DOX-Fol-treated group. Therefore, the SpHL-DOX-Fol enhance the antitumor activity, possibly due to the higher and faster liposomes tumor uptake as showed in biodistribution studies, suggesting that FR-mediated SpHL-DOX-Fol endocytosis carries DOX directly to the nucleus which may enhance the intracellular effects by topoisomerase II inhibition, resulting in cell death [47,48].

DOX-induced cardiac injury is characterized by vacuolization of cardiomyocytes and cell hyalinization. This lesion is responsible for T wave dispersion with consequent prolongation of QT and QTc interval on the ECG records in rodents [49,50]. In this study, QT and QTc intervals dispersion, an expected DOX cardiac toxic effect [5], was not observed in SpHL-DOX or SpHL-DOX-Fol-treated animals during all ECG records, despite some vacuolization areas in histology analysis. In

contrast, mice treated with free DOX showed a significant cardiotoxicity, expressed by prolongation of QT and QTc intervals. DOX encapsulation in nanosystems, including liposomes, is an efficient strategy to avoid the DOX cardiotoxicity [51]. This behavior was demonstrated previously by our research group after administration of a single dose of SpHL-DOX (15 mg/kg) and the coating with folate had no influence in cardiotoxicity profile of SpHL-DOX, highlighting the cardiac safety profile of SpHL-DOX-Fol even after administration of repeated doses [11].

5. Conclusions

In this study, we develeoped and characterized folate-coated, long-circulating and pH-sensitive liposomes containing DOX (SpHL-DOX-Fol). This novel multifunctional nanoplatform presented higher tumor uptake and antitumor activity. Moreover, SpHL-DOX-Fol showed lower cardiotoxicity than free DOX after multiple intravenous administration. These data support further preclinical development of SpHL-DOX-Fol as a promising drug delivery system for the treatment of breast cancer.

Declaration of Competing Interest

The authors declare that they have no conflict of interests.

Acknowledgements

The authors would like to thank Centro de Aquisição e Processamento de Imagens da UFMG (CAPI/UFMG - Brazil) for confocal microscopy images acquisition and Centro de Microscopia (UFMG - Brazil) for TEM images acquisition. This work was supported by Fundação de Amparo à Pesquisa do Estado de Minas Gerais (FAPEMIG - Brazil), Conselho Nacional de Desenvolvimento Científico e Tecnológico (CNPq - Brazil), and Coordenação de Aperfeiçoamento de Pessoal de Nível Superior (CAPES - Brazil). DMT is supported by the Redox Signaling COBRE and Analytical Redox Biochemistry Core (USA).

References

[1] S. Al-Mahmood, J. Sapiezynski, O.B. Garbuzenko, T. Minko, Metastatic and triple-negative breast cancer: challenges and treatment options, Drug Deliv. Transl. Res. 8 (2018) 1483–1507.
[2] R.L. Siegel, K.D. Miller, A. Jemal, Cancer statistics, 2019, CA Cancer J. Clin. 69 (2019) 7–34.
[3] R.M. Damiani, D.J. Moura, C.M. Viau, R.A. Caceres, J.A.P. Henriques, J. Saffi, Pathways of cardiac toxicity: comparison between chemotherapeutic drugs doxorubicin and mitoxantrone, Arch. Toxicol. 90 (2016) 2063–2076.
[4] Y.L. Franco, T.R. Vaidya, S. Ait-Oudhia, S1, Anticancer and cardio-protective effects of liposomal doxorubicin in the treatment of breast cancer, Breast Cancer 10 (2018) 131–141.
[5] J. Wojtacki, E. Lewicka-Nowak, K. Leśniewski-Kmak, Anthracycline-induced cardiotoxicity: clinical course, risk factors, pathogenesis, detection and prevention - review of the literature, Med. Sci. Monit. 6 (2000) 411–420.
[6] P. Veronese, D.T. Hachul, M.I. Scanavacca, L.A. Hajjar, T.C. Wu, L. Sacilotto, C. Veronese, F.C.D.C. Darrieux, Effects of anthracycline, cyclophosphamide and taxane chemotherapy on QTc measurements in patients with breast cancer, PLoS One 13 (2018) 1–10.
[7] E.A. Leite, C.M. Souza, A.D. Carvalho-Júnior, L.G. Coelho, A.M. Lana, G.D. Cassali, M.C. Oliveira, Encapsulation of cisplatin in long-circulating and pH-sensitive liposomes improves its antitumor effect and reduces acute toxicity, Int. J. Nanomedicine 7 (2012) 5259–5269.
[8] J.O. Silva, R.S. Fernandes, S.C. Lopes, V.N. Cardoso, E.A. Leite, G.D. Cassali, M.C. Marzola, D. Rubello, M.C. Oliveira, A.L. de Barros, pH-Sensitive, long-circulating liposomes as an alternative tool to deliver doxorubicin into tumors: a feasibility animal study, Mol. Imaging Biol. 18 (2016) 898–904.
[9] D. Dos Santos, B.L. Ferreira, Jesus de Oliveira Pinto, V. Kumar, V.N. Cardoso, S.O. Fernandes, C.M. Souza, G.D. Cassali, A. Moore, D.E. Sosnovik, C.T. Farrar, E.A. Leite, R.J. Alves, M.C. de Oliveira, A.R. Guimarães, P. Caravan, Evaluation of antitumor activity and cardiac toxicity of a bone-targeted ph-sensitive liposomal formulation in a bone metastasis tumor model in mice, Nanomedicine 13 (2017) 1693–1701.
[10] M.S. Franco, M.C. Roque, A.L.B. de Barros, J. de Oliveira Silva, G.D. Cassali, M.C. Oliveira, Investigation of the antitumor activity and toxicity of long-circulating and fusogenic liposomes co-encapsulating paclitaxel and doxorubicin in a murine breast cancer animal model, Biomed. Pharmacother. 109 (2019) 1728–1739.
[11] J. de Oliveira Silva, S.E.M. Miranda, E.A. Leite, A. de Paula Sabino, K.B.G. Borges, V.N. Cardoso, G.D. Cassali, A.G. Guimarães, M.C. Oliveira, A.L.B. de Barros, Toxicological study of a new doxorubicin-loaded pH-sensitive liposome: a preclinical approach, Toxicol. Appl. Pharmacol. 352 (2018) 162–169.
[12] Y. Xia, M. Fang, J. Dong, C. Xu, Z. Liao, P. Ning, Q. Zeng, pH sensitive liposomes delivering tariquidar and doxorubicin to overcome multidrug resistance of resistant ovarian cancer cells, Colloids Surf. B Biointerfaces 170 (2018) 514–520.
[13] L.O.F. Monteiro, Â. Malachias, G. Pound-Lana, R. Magalhães-Paniago, V.C.F. Mosqueira, M.C. Oliveira, A.L.B. de Barros, E.A. Leite EA, Paclitaxel-loaded pH-sensitive liposome: new insights on structural and physicochemical characterization, Langmuir 34 (2018) 5728–5737.
[14] M.C. De Oliveira, V. Rosilio, P. Lesieur, C. Bourgaux, P. Couvreur, M. Ollivon, C. Dubernet, pH-sensitive liposomes as a carrier for oligonucleotide in excess water, Biophys. Chem. 87 (2000) 127–137.
[15] A.L. de Barros, L.D. Mota, D.C. Soares, C.M. de Souza, G.D. Cassali, M.C. Oliveira, V.N. Cardoso, Long-circulating, pH-sensitive liposomes versus long-circulating, non-pH-sensitive liposomes as a delivery system for tumor identification, J. Biomed. Nanotechnol. 9 (2013) 1636–1643.
[16] A.L. de Barros, L.D. Mota, M.M. Coelho, N.C. Corrêa, A.M. De Góes, M.C. Oliveira, V.N. Cardoso, Bombesin encapsulated in long-circulating pH-sensitive liposomes as a radiotracer for breast tumor identification, J. Biomed. Nanotechnol. 11 (2015) 342–350.
[17] D. Chang, Y. Gao, L. Wang, G. Liu, Y. Chen, T. Wang, W. Tao, L. Mei, L. Huang, X. Zeng, Polydopamine-based surface modification of mesoporous silica nanoparticles as pH-sensitive drug delivery vehicles for cancer therapy, Colloids Interface Sci. Commun. 463 (2016) 279–287.
[18] W. Cheng, C. Liang, X. Wang, H. Tsai, G. Liu, Y. Peng, J. Nie, L. Huang, L. Mei, X. Zeng, A drug-self-gated and tumor microenvironment-responsive mesoporous silica vehicle: "four-in-one" versatile nanomedicine for targeted multidrug-resistant cancer therapy, Nanoscale 9 (2017) 17063–17073.
[19] S. Liu, J. Pan, J. Liu, Y. Ma, F. Qiu, L. Mei, X. Zeng, G. Pan, Dynamically PEGylated and borate-coordination-polymer-coated polydopamine nanoparticles for synergetic tumor-targeted, chemo-photothermal combination therapy, Small 14 (2018) 1–12.
[20] M. Alavi, M. Hamidi, Passive and active targeting in cancer therapy by liposomes and lipid nanoparticles, Drug Metab. Pers. Ther. 34 (2019) 1–8.
[21] M. Alibolandi, K. Abnous, F. Hadizadeh, S.M. Taghdisi, F. Alabdollah, M. Mohammadi, H. Nassirli, M. Ramezani, Dextran-poly lactide-co-glycolide polymersomes decorated with folate-antennae for targeted delivery of docetaxel to breast adenocarcinima in vitro and in vivo, J. Control. Release 241 (2016) 45–56.
[22] M.V. Barbosa, L.O. Monteiro, G. Carneiro, A.R. Malagutti, J.M. Vilela, M.S. Andrade, M.C. Oliveira, A.D. Carvalho-Junior, E.A. Leite, Experimental design of a liposomal lipid system: a potential strategy for paclitaxel-based breast cancer treatment, Colloids Surf. B Biointerfaces 136 (2015) 553–561.
[23] L.O.F. Monteiro, R.S. Fernandes, C.M.R. Oda, S.C. Lopes, D.M. Townsend, V.N. Cardoso, M.C. Oliveira, E.A. Leite, D. Rubello, A.L.B. de Barros, Paclitaxel-loaded folate-coated long circulating and pH-sensitive liposomes as a potential drug delivery system: a biodistribution study, Biomed. Pharmacother. 97 (2018) 489–495.
[24] A.D. Bangham, M.M. Standish, J.C. Watkins, Diffusion of univalent ions across the lamellae of swollen phospholipids, J. Mol. Biol. 13 (1965) 238–252.
[25] V. Vichai, K. Kirtikara, Sulforhodamine B colorimetric assay for cytotoxicity screening, Nat. Protoc. 1 (2006) 1112–1116.
[26] C.C.F. Faraco, J.A.Q.A. Faria, M. Kunrath-Lima, M.C. Miranda, M.I.A. de Melo, A.D.F. Ferreira, M.A. Rodrigues, D.A. Gomes, Translocation of Epidermal Growth Factor (EGF) to the nucleus has distinct kinetics between adipose tissue-derived mesenchymal stem cells and a mesenchymal cancer cell lineage, J. Struct. Biol. 202 (2018) 61–69.
[27] C.M.R. Oda, R.S. Fernandes, S.C. de Araújo Lopes, M.C. de Oliveira, V.N. Cardoso, D.M. Santos, A.M. de Castro Pimenta, Â. Malachias, R. Paniago, D.M. Townsend, P.M. Colletti, D. Rubello, R.J. Alves, A.L.B. de Barros, E.A. Leite, Synthesis, characterization and radiolabeling of polymeric nano-micelles as a platform for tumor delivering, Biomed. Pharmacother. 89 (2017) 268–275.
[28] A. Anisiewicz, A. Pawlik, B. Filip-Psurska, E. Turlej, S. Dzimira, M. Milczarek, K. Gdesz, D. Papiernik, J. Jarosz, D. Kłopotowska, A. Kutner, A. Mazur, J. Wietrzyk, Unfavorable effect of calcitriol and its low-calcemic analogs on metastasis of 4T1 mouse mammary gland cancer, Int. J. Oncol. 52 (2018) 103–126.
[29] A.F.M. Botelho, M.S. Oliveira, B. Soto-Blanco, M.M. Melo, Computerized electrocardiography in healthy conscious Guinea Pigs (*Cavia Porcellus*), Pesqui. Vet. Bras. 36 (2016) 1203–1208.
[30] H.C. Thode, Testing for Normality, first ed., Oxfordshire, 2002.
[31] X. Sun, X. Yan, O. Jacobson, W. Sun, Z. Wang, X. Tong, Y. Xia, D. Ling, X. Chen, Improved tumor uptake by optimizing liposome based RES blockade strategy, Theranostics 7 (2017) 319–328.
[32] F. Tavassolian, G. Kamalinia, H. Rouhani, M. Amini, S.N. Ostad, M.R. Khoshayand, F. Atyabi, M.R. Tehrani, R. Dinarvand, Targeted poly (L-γ-glutamyl glutamine) nanoparticles of docetaxel against folate over-expressed breast cancer cells, Int. J. Pharm. 467 (2014) 123–138.
[33] Y. Patil, H. Shmeeda, Y. Amitay, P. Ohana, S. Kumar, A. Gabizon, Targeting of folate-conjugated liposomes with co-entrapped drugs to prostate cancer cells via prostate-specific membrane antigen (PSMA), Nanomedicine 14 (2018) 1407–1416.
[34] Z.C. Soe, R.K. Thapa, W. Ou, M. Gautam, H.T. Nguyen, S.G. Jin, S.K. Ku, K.T. Oh, H.G. Choi, C.S. Yong, J.O. Kim, Folate receptor-mediated celastrol and irinotecan combination delivery using liposomes for effective chemotherapy, Colloids Surf. B

Biointerfaces 170 (2018) 718–728.
[35] A.K. Deshantri, A. Varela Moreira, V. Ecker, S.N. Mandhane, R.M. Schiffelers, M. Buchner, M.H.A.M. Fens, Nanomedicines for the treatment of hematological malignancies, J. Control. Release 287 (2018) 194–215.
[36] D.S. Ferreira, S.D. Faria, S.C. Lopes, C.S. Teixeira, Â. Malachias, R. Magalhães-Paniago, J.D. de Souza Filho, B.L. Oliveira, A.R. Guimarães, P. Caravan, L.A. Ferreira, R.J. Alves, M.C. Oliveira, Development of a bone-targeted pH-sensitive liposomal formulation containing doxorubicin: physicochemical characterization, cytotoxicity, and biodistribution evaluation in a mouse model of bone metastasis, Int. J. Nanomed. 11 (2016) 3737–3751.
[37] M.C. Woodle, L.R. Collins, E. Sponsler, N. Kossovsky, D. Papahadjopoulos, F.J. Martin, Sterically stabilized liposomes. Reduction in electrophoretic mobility but not electrostatic surface potential, Biophys. J. 61 (1992) 902–910.
[38] S.C.A. Lopes, M.V.M. Novais, C.T. Salviano, K. Honorato-Sampaio, M. Tadeu Pereira, L.A. Ferreira, F.C. Braga, M.C. Oliveira, Preparation, physicochemical characterization, and cell viability evaluation of long-circulating and pH-sensitive liposomes containing ursolic acid, Biomed Res. Int. 2013 (2013) 1–7.
[39] R.S. Fernandes, J.O. Silva, H.A. Seabra, M.S. Oliveira, V.M. Carregal, J.M.C. Vilela, M.S. Andrade, D.M. Townsend, P.M. Colletti, E.A. Leite, V.N. Cardoso, L.A.M. Ferreira, D. Rubello, A.L.B. Barros, A- Tocopherol succinate loaded nanostructed lipid carriers improves antitumor activity of doxorubicin in breast cancer models in vivo, Biomed. Pharmacother. 103 (2018) 1348–1354.
[40] J. Hong, Z. Sun, Y. Li, Y. Guo, Y. Liao, M. Liu, X. Wang, Folate-modified Annonaceous acetogenins nanosuspensions and their improved antitumor efficacy, Int. J. Nanomedicine 12 (2017) 5053–5067.
[41] V.D. Nguyen, H.K. Min, C.S. Kim, J. Han, J.O. Park, E. Choi, Folate receptor-targeted liposomal nanocomplex for effective synergistic photothermal-chemotherapy of breast cancer in vivo, Colloids Surf. B Biointerfaces 173 (2018) 539–548.
[42] J.G. Rosch, A.L. Brown, A.N. DuRoss, E.L. DuRoss, G. Sahay, C. Sun, Nanoalginates via Inverse-Micelle synthesis: doxorubicin-encapsulation and breast cancer cytotoxicity, Nanoscale Res. Lett. 13 (2018) 1–10.
[43] S.A. DuPré, D. Redelman, K.W. Hunter, The mouse mammary carcinoma 4T1: characterization of the cellular landscape of primary tumours and metastatic tumour foci, Int. J. Exp. Pathol. 88 (2007) 351–360.
[44] H. Deng, K. Song, X. Zhao, Y. Li, F. Wang, J. Zhang, A. Dong, Z. Qin, Tumor microenvironment activated membrane fusogenic liposome with speedy antibody and doxorubicin delivery for synergistic treatment of metastatic tumors, ACS Appl. Mater. Interfaces 9 (2017) 9315–9326.
[45] X. Kang, Z. Zheng, Z. Liu, H. Wang, Y. Zhao, W. Zhang, M. Shi, Y. He, Y. Cao, Q. Xu, C. Peng, Y. Huang, Liposomal codelivery of doxorubicin and andrographolide inhibits breast cancer growth and metastasis, Mol. Pharm. 15 (2018) 1618–1626.
[46] H. Abumanhal-Masarweh, L. Koren, A. Zinger, Z. Yaari, N. Krinsky, G. Kaneti, N. Dahan, Y. Lupu-Haber, E. Suss-Toby, E. Weiss-Messer, M.6 Schlesinger-Laufer, J.2 Shainsky-Roitman, A.7 Schroeder, Sodium bicarbonate nanoparticles modulate the tumor pH and enhance the cellular uptake of doxorubicin, J. Control. Release 28 (2019) 1–13.
[47] S.K. Sriraman, G. Salzano, C. Sarisozen, V. Torchilin, Anti-cancer activity of doxorubicin-loaded liposomes co-modified with transferrin and folic acid, Eur. J. Pharm. Biopharm. 105 (2016) 40–49.
[48] D. Goren, A.T. Horowitz, D. Tzemach, M. Tarshish, S. Zalipsky, A. Gabizon, Nuclear delivery of doxorubicin via folate-targeted liposomes with bypass of multidrug-resistance efflux pump, Clin. Cancer Res. 6 (2000) 1949–1957.
[49] T. Nousiainen, E. Vanninen, A. Rantala, E. Jantunen, J. Hartikainen, QT dispersion and late potentials during doxorubicin therapy for non-Hodgkin's lymphoma, J. Intern. Med. 245 (1999) 359–364.
[50] K. Razavi-Azarkhiavi, A.H. Jafarian, K. Abnous, B.M. Razavi, K. Shirani, M. Zeinali, M.R. Jaafari, G. Karimi, The comparison of biodistribution, efficacy and toxicity of two PEGylated liposomal doxorubicin formulations in mice bearing C-26 Colon carcinoma: a preclinical study, Drug Res. 66 (2016) 330–336.
[51] M. Alibolandi, K. Abnous, M. Mohammadi, F. Hadizadeh, F. Sadeghi, S. Taghavi, M.R. Jaafari, M. Ramezani, Extensive preclinical investigation of polymersomal formulation of doxorubicin versus Doxil-mimic formulation, J. Control. Release 28 (2017) 228–236.